Nina Weigert, Anna-Lena Schweiger, Jonas Gross, Marie Matthes, Selim Corbacioglu, Gunhild Sommer* and Tilman Heise*

Detection of a 7SL RNA-derived small non-coding RNA using Molecular Beacons *in vitro* and in cells

https://doi.org/10.1515/hsz-2023-0185
Received April 14, 2023; accepted August 11, 2023;
published online August 28, 2023

Abstract: Small non-coding RNAs (sncRNA) are involved in many steps of the gene expression cascade and regulate processing and expression of mRNAs by the formation of ribonucleoprotein complexes (RNP) such as the RNA-induced silencing complex (RISC). By analyzing small RNA Seq data sets, we identified a sncRNA annotated as piR-hsa-1254, which is likely derived from the 3′-end of 7SL RNA2 (RN7SL2), herein referred to as snc7SL RNA. The 7SL RNA is an abundant long non-coding RNA polymerase III transcript and serves as structural component of the cytoplasmic signal recognition particle (SRP). To evaluate a potential functional role of snc7SL RNA, we aimed to define its cellular localization by live cell imaging. Therefore, a Molecular Beacon (MB)-based method was established to compare the subcellular localization of snc7SL RNA with its precursor 7SL RNA. We designed and characterized several MBs *in vitro* and tested those by live cell fluorescence microscopy. Using a multiplex approach, we show that 7SL RNA localizes mainly to the endoplasmic reticulum (ER), as expected for the SRP, whereas snc7SL RNA predominately localizes to the nucleus. This finding suggests a fundamentally different function of 7SL RNA and its derivate snc7SL RNA.

Keywords: sncRNA; molecular beacon; piRNA; live cell; imaging; fluorescence

***Corresponding authors: Gunhild Sommer and Tilman Heise**, Department for Pediatric Hematology, Oncology and Stem Cell Transplantation, University Hospital Regensburg, Franz-Josef-Strauß Allee 11, D-93053 Regensburg, Germany, E-mail: Gunhild.Sommer@klinik.uni-regensburg.de (G. Sommer), Tilman.Heise@klinik.uni-regensburg.de (T. Heise). https://orcid.org/0009-0004-3728-6548 (T. Heise)

Nina Weigert, Anna-Lena Schweiger, Jonas Gross, Marie Matthes and Selim Corbacioglu, Department for Pediatric Hematology, Oncology and Stem Cell Transplantation, University Hospital Regensburg, Franz-Josef-Strauß Allee 11, D-93053 Regensburg, Germany

1 Introduction

Small non-coding RNAs (sncRNA) such as microRNAs (miRNA, ~22 nts), PIWI-interacting RNA (piRNA, ~26–32 nts), and tRNA-derived fragments (tRFs, ~16–35 nts) play a significant role in human disease. Many of those small RNA fragments identified by small RNA Seq projects are openly available and are listed in databases, such as DASHR (https://dashr2.lisanwanglab.org/ (Kuksa et al. 2019; Leung et al. 2016)), piRBase (http://bigdata.ibp.ac.cn/piRBase/ (Wang et al. 2022)) and RNACentral (https://rnacentral.org/ (Consortium 2021)). However, only in a few cases other methods than RNA Seq, such as Northern blot analysis, have validated their existence and for many sncRNAs experimental studies are missing demonstrating their biological function in cells.

Often sncRNAs are involved in the regulation of gene expression by binding to target messenger (m)RNAs and the formation of RNA-induced silencing complex (RISC) (Iwakawa and Tomari 2022). A few well studied examples of sncRNAs have been reported which are derived from larger precursor RNAs such as DR2 Alu repeat-induced small RNAs (riRNAs, ~28–65 nt) derived from DR2 Alu repeat transcripts generated by RNA polymerase III (Hu et al. 2012), tRNA-derived fragments (tRFs) (Dieci et al. 2007; Pekarsky et al. 2023), miR-1983 derived from pre-tRNA-Ile (Hasler and Meister 2016; Hasler et al. 2016), and T3p a telomerase RNA (TERC)-derived small RNA (Fish et al. 2018). Those larger precursor RNAs are part of RNPs with cellular functions such as translation (tRNAs) or telomere length maintenance (TERC). It is expected that sncRNAs are not incorporated to the same RNP as the larger precursor are. Instead, recent studies suggest that sncRNAs gained new functions and are likely to be associated with different RBPs, such as Argonaut clade proteins (Fish et al. 2018; Hasler et al. 2016; Hock and Meister 2008; Hu et al. 2012; Ozata et al. 2019).

The biogenesis of sncRNAs engages the nuclear microprocessor complex Drosha/DGCR8 and cytoplasmic Dicer (Ha and Kim 2014; Izumi et al. 2020; Treiber et al. 2019), or Zucchini and Trimmer (human PNLDC1) essential for the biogenesis of piRNAs in germ line cells (Czech and Hannon 2016; Pippadpally and Venkatesh 2020), and ribonucleases, such as Dicer or Angiogenin required for the biogenesis of

tRFs (Cole et al. 2009; Kumar et al. 2016; Megel et al. 2015; Yamasaki et al. 2009). The precursor RNAs are transcribed by either RNA polymerase (pol) I, II or III. RNA pol III transcripts are initially bound by the La protein (La autoantigen, LARP3, SSB), an abundant mainly nuclear RNA-binding protein (RBP). Due to its RNA chaperone activity the binding of the La protein to the 3′ polyuridine trailer is considered to support proper folding and processing of the precursor molecule (Maraia et al. 2017; Wolin and Cedervall 2002). Therefore, in cells in which the La protein is overexpressed, as seen in many different types of tumor entities (Sommer and Heise 2021), or its functionality is changed due to phosphorylation (Intine et al. 2000; Kuehnert et al. 2015; Schwartz et al. 2004) or sumoylation (Kota et al. 2018; van Niekerk et al. 2007), the normal RNA pol III transcript maturation pathway might be impaired. In these situations RNA pol III transcript derived sncRNAs might be generated. As example, in cell in which the La protein is experimentally depleted the normal maturation of the RNA pol III precursor transcripts is disturbed and tRNA-derived miRNAs can be detected (Hasler et al. 2016) and global miRNA biogenesis is impaired (Liang et al. 2013; Liu et al. 2011).

By reviewing small RNA Seq data sets and the database piRBase, we identified a 32 nucleotides long RNA molecule annotated as piR-hsa-1254 (DQ571003, piR31115) with complete homology to the 3′-end of 7SL RNA – referred herein as snc7SL RNA. Differential expression of this snc7SL RNA has been described in neuroblatoma and breast cancer cell lines (Hashim et al. 2014; Roy and Mallick 2018). The 7SL RNA is an architectural long non-coding RNA incorporated into the signal recognition particle associated with the endoplasmatic reticulum (ER). In the course of studying a potential biological function of the snc7SL RNA, we aimed to define its cellular localization. Therefore, we designed and characterized several Molecular Beacons (MB) (Mao et al. 2020a; Tyagi and Kramer 1996); *in vitro* and tested those in live cells. Using a multiplex approach, we showed by live cell fluorescence microscopy that the 7SL RNA localizes mainly to the ER in the cytoplasm, as expected for the SRP, but that snc7SL RNA predominantly localizes to the nucleus. This differential localization suggests a fundamental different function of 7SL RNA and its processing product snc7SL RNA.

2 Results

2.1 Molecular Beacon design and characterization *in vitro*

To unveil the cellular localization of endogenous snc7SL RNA we designed and characterized several Molecular Beacons (MB). The principle of a MB assay lays in the formation of a stem formed between the 5′- and 3′-end of a DNA oligonucleotide (Tyagi and Kramer 1996). In case of MBs described herein, the 5′-end is linked to a fluorophore (FAM or Cy5) whereas the 3′-end is linked to a quencher (DAB or BHQ2). As long as the stem is formed, the 5′- and 3′-ends are in close proximity, the quencher absorbs the energy of the excited fluorophore and prevents emission of fluorescence light upon excitation. Hence, the stability of the stem is a critical parameter. In case the stem is very weak, spontaneous strand separation occurs and fluorescence light emission causes a strong background fluorescence signal (F_{back}). On the other hand, if the stem is very stable the fluorescence light emission in presence of the target molecule is diminutive indicating a low sensitivity. To calculate the assay window (AW = F_{max}–F_{back}) for the various MBs tested herein, we determined the maximal fluorescence (F_{max}) by incubating the MBs in 50 % formamide and subtracted the background fluorescence signal. Hence, an optimal MB generates a low background signal, has a large assay window (F_{max}–F_{back}) and is highly sensitive and specific in detecting the target sequence.

Considering the MB criteria mentioned above, we designed seven MBs of different stem stability (MBsnc7SL, MBsnc7SL-S, MBsnc7SL-Mut, MBcon, MBcon-S, MB7SL, MB6145-S) and complementarity to four target RNA molecules: (1) snc7SL RNA (piR-has-1254; DQ571003), (2) synthetic control RNA (con-target, reverse sequence of snc7SL RNA), (3) 7SL RNA (RN7SL2; NR_027260.1), and (4) as positive control piR-has-6145 (DQ575882), another endogenously expressed sncRNA (Figure 1A and B). Bold capital letters indicate MB sequences complementary to the respective target RNA sequence (Figure 1B). The number of guanine:cytosine (G:C) base pairs of the stem varies between six (MBsnc7SL-S, MBcon-S, MB6145-S), five (MBsnc7SL-Mut), and four (MBsnc7SL, MB7SL, MBcon) (Figures 1B and 2). In case of MBsnc7SL-Mut, five G:C base pairs are closing the structure, two additional adenosines flank the G:C base pairs, five nucleotides were deleted to shorten the complementary sequence to snc7SL target RNA and three cytosines were substituted by adenosines to weaken the base pairing with the snc7SL target RNA. As mentioned above, snc7SL RNA is derived from the larger 7SL RNA and the target sequences for MBsnc7SL and MB7SL are shown in the scheme of the predicted folding of RNA7SL (Figure 1C; Andersen et al. 2006; Bovia and Strub 1996).

We used the DNA folding form at the UNAFold web server (http://www.unafold.org/; Zuker 2003) to calculate the two dimensional folding of each MB and the stability of those structures (ΔG values). The predicted structures with the

A) Target Sequence:

sncRNA 7SL	5′-AGCCUGAGCAACAUAGCGAGACCCCGUCUCU-3′
con-target	5′-AUCUCUGCCCCAGAGCGAUACAACGAGUCCG-3′
7SL RNA	5′-AGUUCUGGGCUGUAGUGCGCUAUGCCGAUC-3′
piR-has-6145	5′-UCCGUAGUGUAGUGGUUAUCACGUUCGCCUCA-3′

B) Molecular beacons:

MBsnc7SL	5′-FAM- cgcg**AGAGACGGGGTCTCGCTATGTTGCTCAGGCT**cgcg -3′-DAB
MBsnc7SL-S	5′-FAM-cgcgcg**AGAGACGGGGTCTCGCTATGTTGCTCAGGCT**cgcgcg -3′-DAB
MBsnc7SL-Mut	5′-FAM-cgcgca**----ACGGGGTaTCGaTATGTTGCTCAGGC-a**gcgcg -3′-DAB
MBcon	5′-FAM-cgcg**TCGGACTCGTTGTATCGCTCTGGGGCAGAGAT**cgcg -3′-DAB
MBcon-S	5′-FAM-cgcgcg**TCGGACTCGTTGTATCGCTCTGGGGCAGAGAT**cgcgcg-3′-DAB
MB7SL	5′-Cy5-cgcga**GATCGGCATAGCGCACTACAGCCCAGAACT**cgcg -3′-BHQ2
MB6145	5′-FAM-cgcgcg**TGAGGCGAACGTGATAACCACTACACTACGGA**cgcgcg-3′-DAB

C)

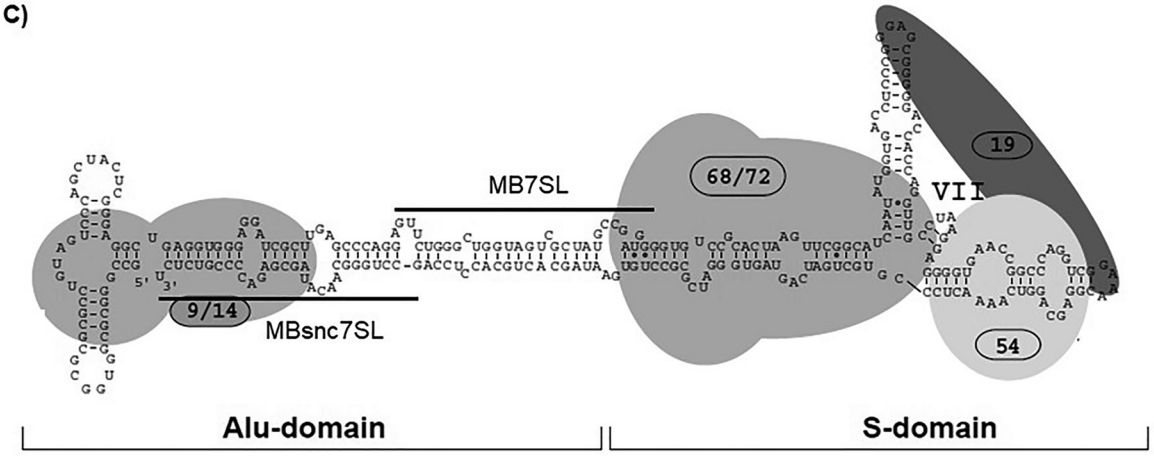

Figure 1: Sequences of Molecular Beacons and their target RNAs. A) RNA sequences targeted by Molecular Beacons (MB). B) MBs are 5′-labeled with fluorophores (FAM or Cy5) and quenchers (DAB or BHQ) are linked to the 3′-end. MB sequences (DNA) complementary to the respective target RNA (bold). In MBsnc7SL-Mut five nucleotides are deleted (–) and three nucleotides are changed (small letters underlined). MB with –S (stable) = more guanine:cytosine (G:C) base pairs. FAM, fluorescein; DAB, dabcyl quencher; Cy5, cyanine 5; BHQ, black hole quencher. C) Structure of the 7SL RNA molecule and binding sites of the six signal recognition particle proteins 72, 68, 54, 19, 14, 9 (adapted from (Bovia and Strub 1996)). The target sequences for MB7SL and MBsnc7SL are indicated by black lines.

lowest ΔG values are shown (Figure 2). In all structures the stem formed as expected, based on the G:C base pairs, positioning the fluorophore and quencher in close proximity. All MBs – except MB7SL– had a large single stranded loop area harboring the complementary sequence of the target molecule. Furthermore, all MBs with six G:C base pairs were more stable than those with just five or four G:C base pairs. MB7SL formed a longer stem due to of G:C base pairs formed by complementarity within the target sequence (Figure 2D).

Since it was planned to test the MBs in cell culture experiments, their stability at 37 °C was an important test parameter. We characterized the stability of the MBs by measuring the background fluorescence (F_{back}) in different reaction buffers and at different temperatures (data not shown). The lowest F_{back} value for all MBs was measured in the ICN buffer (10 mM Tris/HCl, pH 7.5, 100 mM KCl, 10 mM NaCl, 0.75 mM $MgCl_2$, 0.0001 % NP40) at 37 °C. Therefore, all *in vitro* experiments were performed in ICN buffer. Next, we determined F_{back} for all MBs at different concentrations (5000 nM, 1000 nM, 40 nM (data not shown)) and 200 nM in ICN buffer over time at 37 °C. After 10 min we measured a low and stable F_{back} signal for all MBs at a concentration of 200 nM (Figure 3A) or 100 nM (Supplementary Table 1A). To determine the maximal fluorescence (F_{max}) of 200 nM (Figure 3A, *+F*) or 100 nM (Supplementary Table 1A) FAM-labeled MBs were incubated in 50 % formamide (*F*) over time at 37 °C. By calculating the assay window (AW = F_{max}–F_{back}) after 40 min at 37 °C, a 3- to 4-fold increase in fluorescence was determined for all FAM-labeled MBs (200 nM). Although relative fluorescence units (RFU) determined for the Cy5-labled MB7SL were lower compared to the RFUs measured for the FAM-MBs, a low F_{back} and a 5-fold higher F_{max} was determined at a concentration of 200 nM (Figure 3B) or 100 nM MB7SL (Supplementary Table 1A and B).

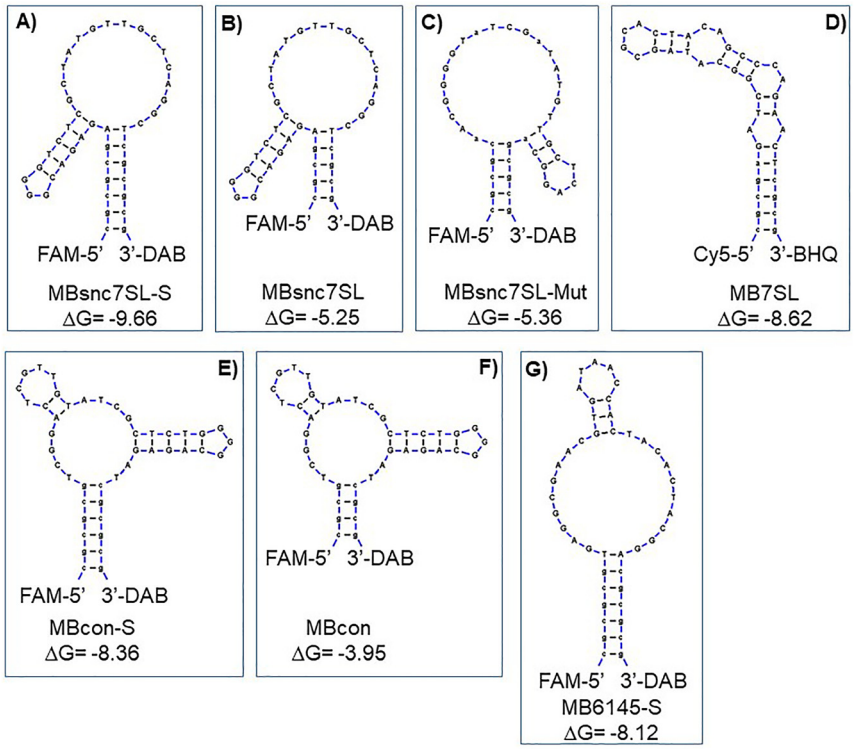

Figure 2: Predicted structures and ΔG values of Molecular Beacons. A) MBsnc7SL-S, B) MBsnc7SL, C) MBsnc7SL-Mut, D) MB7SL, E) MBcon-S, F) MBcon, G) MB6145-S. Structures of DNA Molecular Beacons (MBs) were predicted and ΔG values calculated using DNA fold (http://www.unafold.org (Zuker 2003)). CT files (connectivity table) containing secondary structure information were imported into jViz. RNA 4.0 (http://jviz.cs.sfu.ca/). S = more guanine:cytosine (G:C) base pairs, Mut = deletions or mutations in the snc7SL RNA target sequence. FAM, fluorescein; DAB, dabcyl quencher; Cy5, cyanine 5; BHQ, black hole quencher.

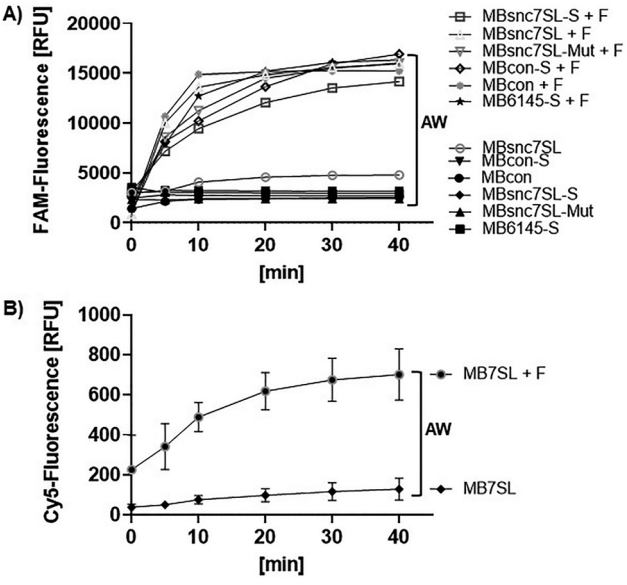

Figure 3: Background (F_{back}) and maximal fluorescence (F_{max}) of Molecular Beacons. A) To determine the background (F_{back}) and maximal (F_{max}) fluorescence, 200 nM of various Molecular Beacons (MBs) were incubated with and without 50 % formamide (+*F*) in ICN buffer over time at 37 °C. FAM-fluorescence was recorded at time point 0, 10, 20, 30, 40 min. *n* = 3; AW, assay window. B) To determine F_{back} and F_{max} of MB7SL, 200 nM were incubated with and without 50 % formamide (+*F*) in ICN buffer over time at 37 °C. Cy5-fluorescence was recorded at time point 0, 10, 20, 30, 40 min. *n* = 3; AW, assay window.

To test the amount of target molecules required for activation of the various MBs, we titrated concentration of the target molecules (0, 25, 100, 100, 400 nM) referred to as con-target RNA, 7SL-target DNA, or snc7SL-target RNA into reactions containing 100 nM MB. None of the MBs were activated at the lowest target molecule concentration of 25 nM. However, 100 nM of the control target RNA (con-target RNA) was sufficient to reach almost F_{max} levels (Figure 4A, Supplementary Table 1A and B). Higher concentrations of con-target RNA reached earlier a plateau but were not reaching higher fluorescence levels as with 100 nM. These findings show that 100 nM MBcon (ΔG = −3.95) is almost maximal open (F_{max}) at a concentration of 100 nM of con-target RNA. When testing the more stable MBsnc7SL (ΔG = −5.25) a concentration of 200 nM of snc7SL target RNA was sufficient to reach a plateau near F_{max}. A concentration of 100 nM snc7SL target RNA opened MBsnc7SL but without reaching F_{max} in the given period of time (Figure 4B, Supplementary Table 1A and B). In case of the stable MB7SL (ΔG = −8.62) even a 4-fold increased concentration of 7SL-target DNA (400 nM) was not sufficient to reach F_{max} in the given time period (Figure 4C, Supplementary Table 1A and B). Taken together, the calculated stability of the MBs correlated with the sensitivity of the MBs and a more stable MB required a higher target molecule concentration for a strong activation.

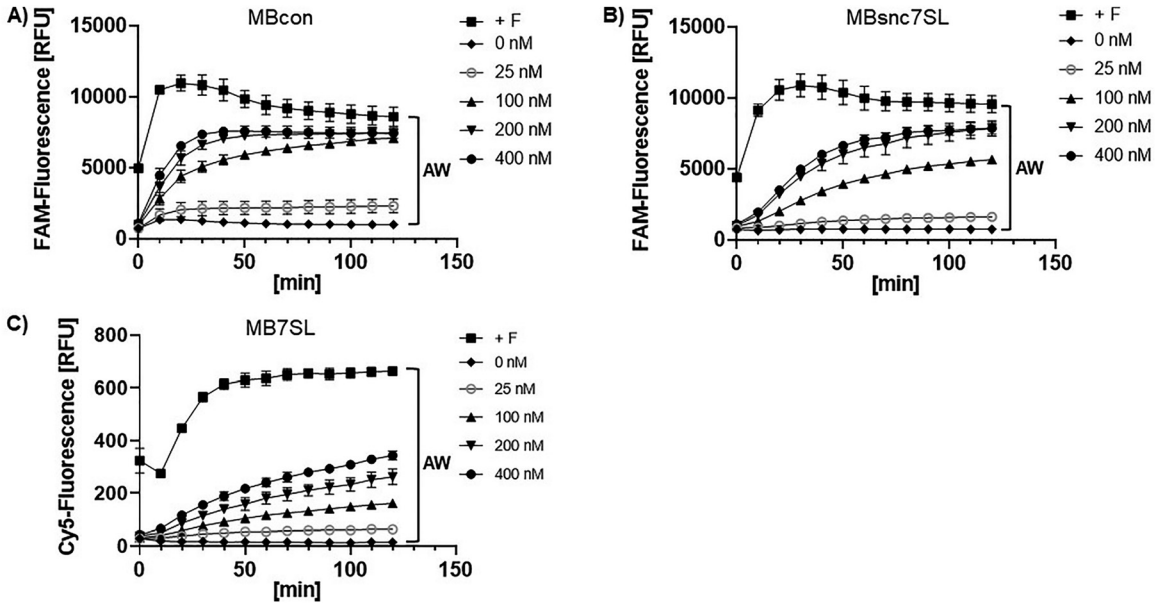

Figure 4: Sensitivity of Molecular Beacons. A) 100 nM of MBcon plus con-target RNA, B) 100 nM of MBsnc7SL plus snc7SL-target RNA, and C) 100 nM of MB7SL plus 7SL-target DNA. MB specificities were tested by incubation of 25, 100, 200, 400 nM of respective target RNA or DNA, without any RNA (F_{back}) or in presence of 50 % formamide (+F, F_{max}). All reactions were assembled on ice, placed in the plate reader preheated to 37 °C. Fluorescence was recorded at 0 and every 10 min for 2 h. n = 2, AW, assay window.

Next, we tested the specificity of the MBs. Therefore, we incubated MBs (100 nM) with 500 nM target molecules. As shown, the fluorescence signal of MBs was only activated by specific target molecules, indicating a high specificity of all MBs tested (Figure 5). The snc7SL-target RNA activated strongly MBsnc7SL (ΔG = −5.25) but only to a small extend MBsnc7SL-S likely because of the increased stability (ΔG = −9.66) of the stem extended by two additional G:C base pairs (Figures 2 and 5A). Interestingly, reducing the complementarity of MBsnc7SL-Mut (ΔG = −5.36) to snc7SL-target RNA by a deletion of five nucleotides and the change of three cytosine residues to adenosine residues was sufficient to prevent its activation by snc7SL-target RNA as also supported by the difference in ΔG values for the MBsnc7SL-Mut:sncRNA7SL-target interaction (ΔG = −6.51) when compared to the MBsncRNA:sncRNA7SL-target interaction (ΔG = −53.13, Figure 6A) underscoring the specificity of the MBsnc7SL (Figure 5A) Con-target RNA activated strongly both con-target RNA specific Molecular Beacons (MBcon-S (ΔG = −8.36), MBcon (ΔG = −3.95)), but activation was not overserved for any other MB (Figure 5B). Similar, MB7SL (ΔG = −8.62) was only activated by its 7SL-target sequence but not, as expected, the snc7SL-target sequence (Figure 5C).

The 7SL RNA is the precursor of all Alu elements (Jurka 2004; Quentin 1994) and 7SL RNA sequences appear as Alu elements in sense or antisense orientation in the 3′UTR of mRNAs (Zhang et al. 2021). To further assess the specificity of the MBsnc7SL, we tested whether those Alu elements represent potential degenerated snc7SL target sequences. We selected six potential target sequences characterized by a relatively high complementarity (few mismatches only) to the snc7SL RNA (Figure 6B). The selected snc7SL target sequences are located in the 3′UTR of Mdm2 mRNA (one sequence), Mdm4 mRNA (two sequences, Mdm4-S1 and -S2), eEF2K mRNA (two sequences, eEF2K-S1 and -S2) and one sequence in KNL1 mRNA. Target molecules with those sequences were tested for their recognition by MBsnc7SL (Figure 6C). Interestingly, whereas the snc7SL target sequence strongly activated (K_m 37.68 nM) the MBsnc7SL, Mdm2- and Mdm4-S1-target sequences were unable to activate MBsnc7SL (Figure 6B and C) even at concentrations of a 4-fold excess (not shown). The second best target molecule was a sequence element derived from Mdm4 (Mdm4-S2, K_m = 77.43 nM) and the remaining three eEFK2-S1, eEFK2-S1 and KNL1 target molecules activated the MBsnc7SL only with high K_m suggesting a low affinity (Figure 6B and C). Using the program RNAcofold (http://rna.tbi.univie.ac.at//cgi-bin/RNAWebSuite/RNAcofold.cgi; Gruber et al. 2008), we calculated ΔG values for the base pairing between the loop sequence of MBsnc7SL and all potential target sequences (Figure 6B). A correlation between low ΔG values, strong MBsnc7SL opening and higher ΔG values and weak or no MBsnc7SL opening was found. In light of previous studies

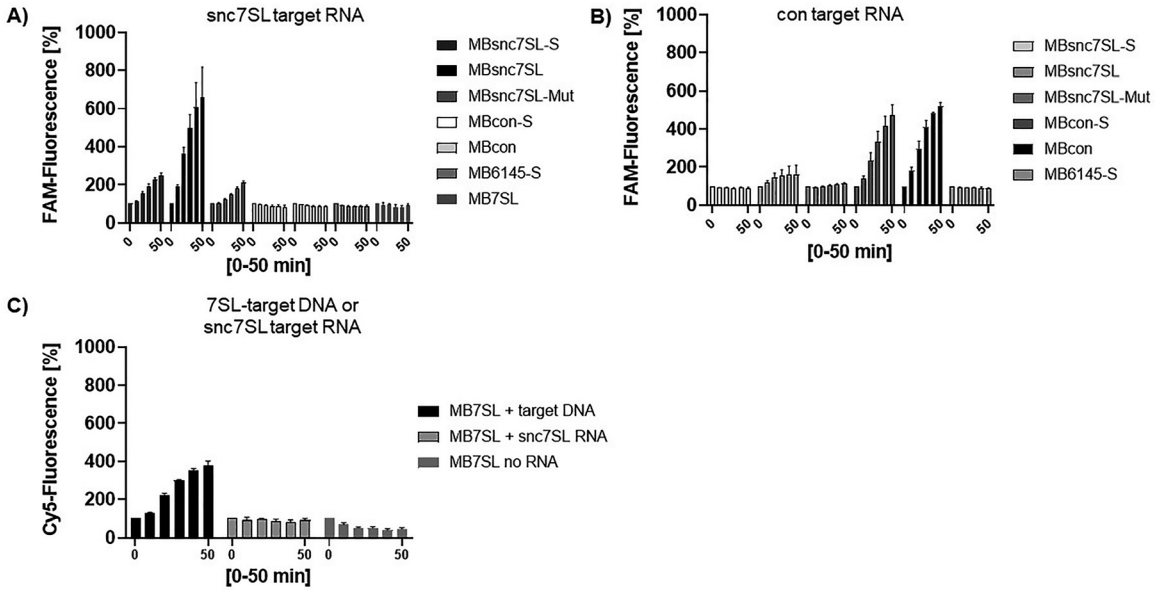

Figure 5: Target specificity of Molecular Beacons. A) 100 nM of MBs were incubated with 500 nM of snc7SL-target RNA. B) 100 nM of MBs were incubated with 500 nM of con-target RNA. C) 100 nM of MB7SL were incubated with 500 nM of 7SL-target DNA, snc7SL-target RNA or without any RNA. All reactions were incubated for 0, 10, 20, 30, 40, 50 min at 37 °C in ICN buffer. n = 3.

A)

MB	MB target DNA	sequence	miss,del,extra	ΔG kcal/mol
MBsncRNA7SL	snc7SL-target	5'-agcctgagcaacatagcgagaccccgtctcta-3'	0	-53,13
MBsncRNA7SL-S	snc7SL-target	5'-agcctgagcaacatagcgagaccccgtctcta-3'	0	-53,13
MBsncRNA7SL-Mut	snc7SL-target	5'-agcctgagcaacatagcgagaccccgtctcta-3'	5 del, 3 miss	-6,51
MBcon	con-target	5'-AUCUCUGCCCCAGAGCGAUACAACGAGUCCGA-3'	0	-56,98
MBcon-S	con-target	5'-AUCUCUGCCCCAGAGCGAUACAACGAGUCCGA-3'	0	-56,98
MB7SL	7SL-target DNA	5'-AGTTCTGGGCTGTAGTGCGCTATGCCGATC-3'	0	-52,00
MB6145	piR-hsa-6145	5'-TCCGTAGTGTAGTGGTTATCACGTTCGCCTCA-3'	0	-56,18

B)

Target name	Target sequence	miss,del,extra	ΔG kcal/mol	Vmax	Km	R squared
snc7SL	5'-agcctgagcaacatagcgagaccccgtctcta	0	-53.13	9416	37.68	0.964
Mdm2	5'--**T*AG*AG***G*TG***-A*TT******-	11 miss, 3 del	-12.13	856.6	1.174	-7.671
Mdm4-S1	5'-*******C*G****G*A**A****A*T*T**	8 miss	-26.62	875.8	3.8E-09	-15.42
Mdm4-S2	5'-******G******A******A*--*T******-*	4 miss, 3 del	-33.49	9762	77.43	0.9066
eEF2K-S1	5'-******G*T**A***G********T******-	4 miss, 1 extra	-39.68	9039	154	0.9348
eEF2K-S2	5'-******G**G***G**T*****T*******G-	6 miss, 1 del	-39.61	5507	110.4	0.8414
KNL1	5'-******G*******G**A*A*****AC*****	6 miss	-33.36	7300	118.6	0.9096

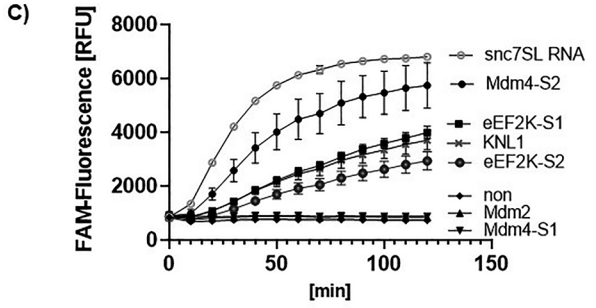

Figure 6: Target specificity of MBsnc7SL. To further test the sequence specificity of MBsnc7SL, degenerated target sequences derived from Alu elements found in the 3′UTR of four mRNAs (Mdm2, Mdm4, eEF2K, KNL1) were chosen. A) ΔG values for the different MB:target sequence interactions are given. B) Sequence of degenerated target sequences: mismatches (mis), deletions (del) or extra (extra) nucleotides are indicated (bold, underlined). V_{max}, K_m and R squared values are given. Grey shaded = no binding, n = 2, ΔG [kcal/mol] for the base pairing between the loop sequence of MBsnc7SL and the target sequence. C) 100 nM MBsnc7SL were incubated without or with 200 nM target DNA in ICN buffer over time at 37 °C. Fluorescence was recorded at 0 time point followed by 10 min intervals for 2 h.

showing that MBs can even discriminate between target molecules based on a single nucleotide substitution (Bonnet et al. 1999; Tyagi et al. 1998), it is not surprising that degenerated snc7SL RNA target sequences let to no or only to a weak MBsnc7SL activation when compared to the 100 % complementary target sequence. Taken together, the *in vitro* studies established that MBsnc7SL has a large assay window and is highly sensitive to alterations in the target sequence indicating a high sequence specificity.

2.2 Detection of snc7SL RNA and 7SL RNA in cells

The MB-based detection of snc7SL RNA and 7SL RNA *in vitro* was highly specific. Next, we aimed to apply MBs to detect and study the subcellular localization of endogenous 7SL RNA and its potential derivate snc7SL RNA. Initially, we plated U2–OS cells into 24-well tissue culture plates, transfected 37.5 nM of MBcon (Figure 7A) or MBsnc7SL (Figure 7B) and took overview pictures 24 h later with the Bio-Rad ZOE cell imager, to test whether it is possible to apply a basic LED-light equipped cell imager to detect MB signals. The control transfection with MBcon showed only very weak signal derived from artificial spots located outside of cells (Figure 7A). In contrast, transfection of MBsnc7SL led to cells with green fluorescence signals mainly localized to the nucleus (Figure 7B, transfection efficiency ~20 %). As clearly visible in the enlarged cells the green fluorescence signal is concentrated in the nucleus with some cytoplasmic staining (Figure 7C and D). In addition, in about ~ 19 % of cells positive for the MBsnc7SL signal fluorescent dots were also found in the cytoplasm (Figure 7D, arrows, 2–3 dots/cell). The nature of these structures is currently under investigation.

Because of the limited resolution of the ZOE instrument, we applied the KEYENCE BZ-X810 fluorescence microscope. Therefore, we plated cells in chambered coverslip wells and transfected the cells with 12.5 nM MBcon, MBsnc7SL, MBsnc7SL-S or MBsnc7SL-Mut. After 24 h, nuclei were stained with DAPI and pictures taken with the KEYENCE BZ-X810 fluorescence microscope. Again, the MBsnc7SL detected snc7SL RNA mainly in the nucleus (Figure 8B, transfection efficiency: ~27 %) and only very weak fluorescence signals were found in control transfections applying MBcon, MBsnc7SL-S or MBsnc7SL-Mut (Figure 8A, C, and D). Those findings are in agreement with our *in vitro* studies showing that the MBsnc7SL only detected specifically the snc7SL target RNA (Figure 6).

To further confirm the predominant nuclear localization of snc7SL RNA, U2–OS cells were transfected with the MBsnc7SL and pictures were taken with a confocal microscope. As shown, the confocal pictures confirmed the predominant nuclear localization of snc7SL RNA (Supplementary Figure 1A). Interestingly, some cytoplasmic snc7SL RNA foci co-localize with DAPI stained DNA foci in the cytoplasm. Those foci might represent micro-nucleoli occurring upon chromosome segregation defects as described by others (De Marco Zompit and Stucki 2021; Naim and Rosselli 2009), however, the characterization of those foci requires a more detailed analysis in future studies. As additional positive control, we designed and tested *in vitro* MB6145-S directed against another endogenously expressed 32 nucleotides long sncRNA, referred to as piR-has-6145

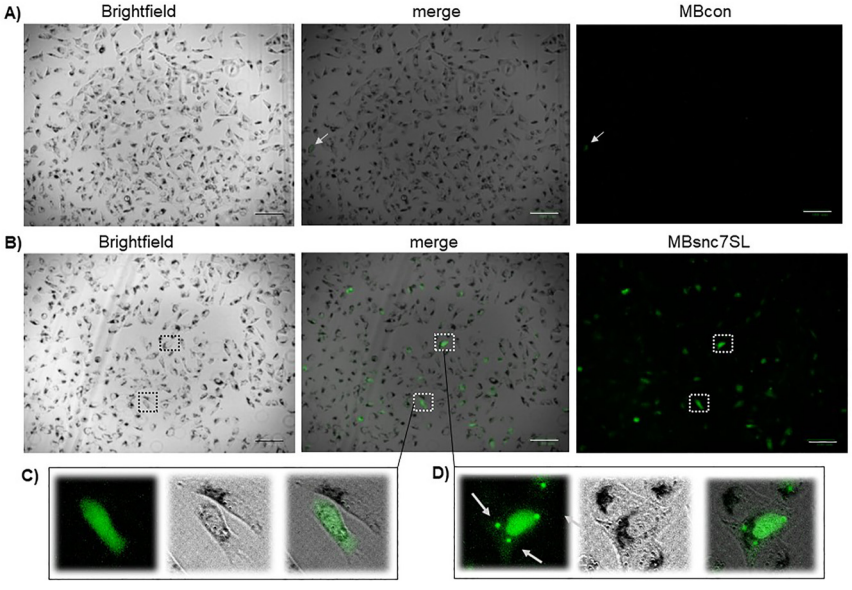

Figure 7: Endogenous sncRNA7SL is predominantly detected in the nucleus of cells. A) As a control U2–OS cells were transfected with 37.5 nM MBcon (arrow indicates some artificial fluorescence signal) or B) sncRNA7SL specific MBsnc7SL. C) and D) shows enlarged cells with a strong MBsnc7SL derived fluorescence signal diffuse in the nucleus and some cytoplasmic foci-like staining. Arrows indicate cytoplasmic foci detected in 19 % of MBsnc7SL positive cells. Scale bar = 100 µm. Pictures were processed using Adobe software package elements.

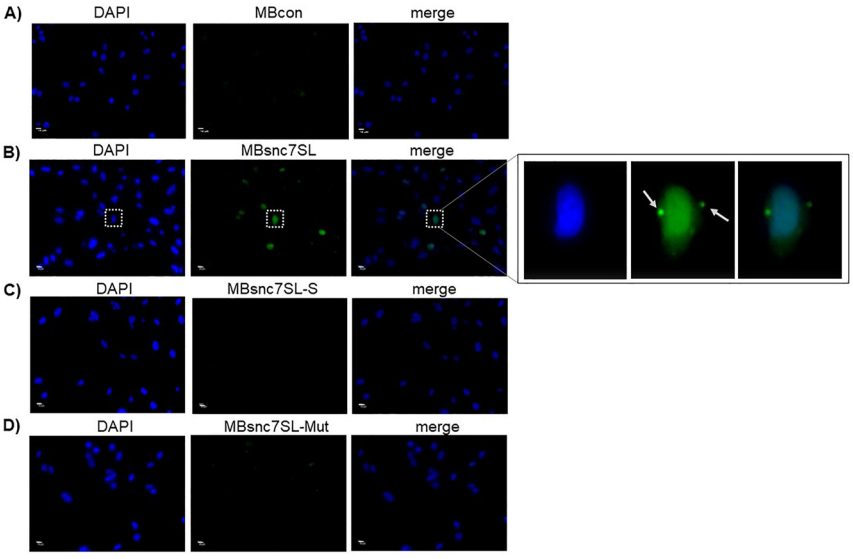

Figure 8: Detection of snc7SL RNA only by MBsnc7SL, but not by MBsnc7SL-S, MBsnc7SL-Mut or MBcon in cells. Cells were transfected with 12.5 nM of A) MBcon, B) MBsnc7SL, C) MBsnc7SL-S, or D) MBsnc7SL-Mut. An enlarged cell is shown in B). Arrows indicate cytoplasmic foci in MBsnc7SL transfected SK–N–SH cells. At 24 h after transfection pictures were taken as Z stacks with a KEYENCE BZ-X810 fluorescence microscope. Magnification = 40×, plan apochromat objective. Scale bar = 10 µM. All pictures were processed using Adobe software package elements.

(Figure 1A and B). Upon transfection of MB6145-S, green fluorescence signal was predominantly detected in the nucleus of the cells (Supplementary Figure 1B). Taken together, only MBs (MBsnc7SL, MB6145-S) with expected cellular target RNAs (snc7SL RNA, piR-has-6145) were opened in cells. Control MBs (MBcon) or MBs with stabilized stem structures (MBsnc7SL-S) or reduced target RNA complementarity (MBsnc7SL-Mut) were not activated in cells.

As mentioned above, the snc7SL RNA is considered to derive from the larger 7SL RNA, which is part of the signal recognition particle (SRP). The SRP localizes to the endoplasmatic reticulum (ER), which is associated with the nuclear envelope (Shibata et al. 2006). Because the snc7SL RNA sequence is homolog to the 3′-end of the 7SL RNA, the MBsnc7SL should detect not only snc7SL RNA but also the 7SL RNA (Figure 1B). In contrast, MB7SL should only detect 7SL RNA and not snc7SL RNA (Figure 1C). Hence, we co-transfected Cy5-labeled MB7SL and FAM-labeled MBsnc7SL into SK–N–SH cells. As shown, the MB7SL was opened and a red signal in close proximity to the nuclear envelope and only a weak nuclear staining was detected (Figure 9A and B, Supplementary Figure 1C). The colocalization of the fluorescence signal of an ER-specific dye with the MB7SL fluorescence signal strongly suggests that the detected 7SL RNA – as part of the SRP – colocalizes with the ER (Figure 9A and B, Supplementary Figure 1C). On the other hand, the MBsnc7SL detected a strong signal in the nucleus (Figure 9A and B). To demonstrate the clearly distinguishable Cy5- and FAM-signals but also the partial colocalization, enlarged cells are shown (Figure 9B). MBsnc7SL detected snc7SL RNA mainly as diffuse signal in the nucleus and some peaks also in the cytoplasm (Figure 9B). In contrast, MB7SL detected 7SL RNA mostly in the cytoplasm and only a faint signal in the nucleus was recorded (Figure 9B). However, the co-localization (yellow signal) of the FAM- and Cy5-signals indicates that MBsnc7SL detects also 7SL RNA to some extend in the cytoplasm (Figure 9B). This observation is further strengthen by line profiles measuring the fluorescence intensity along a drawn line. The main red signal (red line) derived from MB7SL is recorded in the cytoplasm in proximity to the nucleus (blue line) and faint red signal is also detected in the nucleus (Figure 9C). The green line profile is derived from MBsnc7SL and shows the strongest signal in the nucleus but also outside in proximity to the nuclear envelope, suggesting some recognition of the 7SL RNA.

Taken together, herein we report the application of different Molecular Beacons for the intracellular detection of an endogenous large precursor RNA (7SL RNA) and a small processing product (snc7SL RNA) by multiplex live cell microscopy. Interestingly, the MB-based detection revealed a distinct sub-cellular localization of both endogenous RNA molecules.

3 Discussion

Herein, we established a multiplex Molecular Beacon (MB) assay to visualize the localization of 7SL RNA and the 7SL RNA-derived snc7SL RNA in live cells. We started out by characterizing seven different MBs *in vitro* directed against for different target sequences. We found that the design of all MBs caused only a low background fluorescence (F_{back}), signifying a stable stem for a prolonged time at 37 °C in INC buffer, an important aspect for cell-based assays. In addition, we demonstrated the critical importance of stem stability for

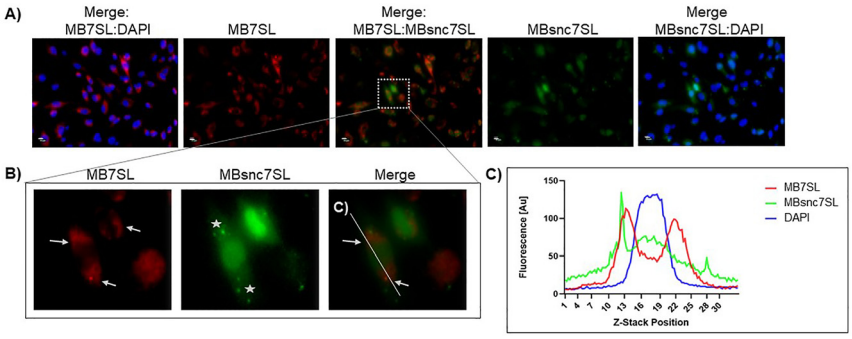

Figure 9: Subcellular localization of 7SL RNA and snc7SL RNA in SKNSH cells. A) Cells were co-transfected with 12.5 nM MB7SL and 12.5 nM MBsnc7SL and the nucleus stained with DAPI. B) Enlarged cells with red signal derived from activated MB7SL show the location of 7SL RNA in distinct areas close to the nuclear envelop (grey arrows). The green FAM signal of activated MBsnc7SL indicates the predominant localization of snc7SL RNA in the nuclei. Colocalization of the FAM and Cy5 signal shows the distinct localization of 7SL RNA outside of the nucleus and the predominant localization of snc7SL RNA within the nucleus. However, some colocalization of both signals were detected (yellow). Stars indicating cytoplasmic foci of unclear nature. C) Line profile. 24 h after transfection pictures were taken as Z stacks with a KEYENCE BZ-X810 fluorescence microscope. Z stack were taken with a 40× magnification. Plan apochromat objective. Scale bar = 10 µM. All pictures were processed using Adobe software package elements.

MBs sensitivity. Two additional G:C base pairs in the stem reduce MBs sensitivity dramatically so that even a five-fold excess of target RNA was not able to open MBsnc7SL-S (seven base pair stem, ΔG = −9.75) when compared to MBsnc7SL (five base pair stem, ΔG = −5.75). This observation is notable, because the principle of a MB lays in the opening of the stem upon target hybridization (Bonnet et al. 1999). In the above example the stability of MB:target duplexes, as determined by applying the T_m calculator CompareTm (https://bioinf.fisica.ufmg.br/app/comparetm.pl; Basilio Barbosa et al. 2019; Ferreira et al. 2019; Weber 2015), between MBsnc7SL and MBsnc7SL-S and its target RNA sequence (ΔG = −42.6, Figure 4) or target DNA sequence (ΔG = −40.5, Figure 6) is much higher than the stability of the stem predicted to form in MBsnc7SL (ΔG = −5.75) or MBsnc7SL-S (ΔG = −9.75). Although stem stability is critical for a low F_{back} and MB sensitivity, other parameters appear to be important for MB opening. For example, MB7SL has an extended stem due to base pairing in the target sequence preventing the formation of an open loop region (Figure 2D). However, MB7SL (ΔG = −8.62) was specifically open at low target concentrations *in vitro* when compared to MBsnc7SL-S (ΔG = −9.66), which opened only at high target concentrations, suggesting that although both MBs are of comparable stability other factors as the target sequence must play a role (Figure 5A and C).

Herein we used target DNA or RNA molecules. Hence, to compare the melting temperatures we calculated the melting temperature for the DNA:RNA duplex (MBsnc7SL:target RNA), DNA:DNA duplex (MBsnc7SL:target DNA), and for the RNA:RNA interaction between a theoretical RNA-based MBsnc7SL and the target RNA applying the T_m calculator CompareTm. As parameters we used a concentration of 100 nM for MBs and 110 mM for cations (Ka^+ and Na^+, see ICN Buffer). The RNA:RNA duplex was most stable (T_m = 88.6072 °C), followed by the DNA:DNA duplex (T_m = 73.633 °C) and the DNA:RNA duplex (T_m = 70.8285 °C). In this context, it is interesting that, although of comparable stability MBcon (ΔG = −3.95) and MBsnc7SL (ΔG = −5.25), our *in vitro* data show that MBcon was opened by the con-target RNA at much lower K_m (K_m = 18.11) when compared to the interaction between MBsnc7SL and its sncRNA7L target RNA (K_m = 62.47) (Supplementary Table 1). This is remarkable, since the calculated T_m values for the MB:target duplex comparing MBcon:con-target RNA (DNA:RNA duplex: T_m = 69.951 °C) with MBsnc7SL:snc7SL–target RNA (DNA:RNA duplex: T_m = 70.8285 °C) were also very similar. Hence, this data suggest that the interaction between DNA MBs and RNA target molecules depends strongly on additional parameters other than melting temperature, MB stability and structure. Additional critical parameter are likely the buffer conditions, concentrations of MBs and target molecules.

In the literature, it is reported that cations have a major impact on duplex formation (Nakano et al. 1999) affecting not only the MB stem stability but also the duplex formation between MB and target molecule. In addition, target molecule concentrations influence the outcome of MB assays as shown herein. Those relationships can be well studied *in vitro*, however, cell-based assays are much more complex due to additional cellular factors impacting the duplex

formation, such as varying salt concentrations, interfering cellular RNA-binding factors and the unknown concentration of the endogenous target RNA.

As already shown by others, MBs can discriminate between a single nucleotide polymorphism in target sequences (Kostrikis et al. 1998; Tyagi et al. 1998). We also observed a pronounced sequence specificity *in vitro*. The deletion of five and the mutagenesis of three out of 32 nucleotides of the complementary target sequence in MBsnc7SL-Mut almost completely prevented the opening of the MB even in presence of a five-fold excess of snc7SL-target RNA. Using the *in vitro* studies reported herein should allow the identification of nucleotides in the target sequences crucial for recognition by MBs.

In addition, MBsnc7SL might not only detect snc7SL RNA but also target sequences present in the 3′UTR of Alu element containing mRNAs in living cells. Therefore, we selected degenerated MBsnc7SL target sequences found in the 3′UTR of several Alu element containing mRNAs and tested the interaction *in vitro*. We show that those degenerated snc7SL-target sequences open the MBsnc7SL only at high concentrations compared to low concentrations of wildtype snc7SL-target sequences sufficient for MB opening. Therefore, it is unlikely that the MBsnc7SL detects degenerated target sequences buried in the 3′UTR of specific mRNA in live cell imaging unless those are highly expressed. However, adapting the MBsnc7SL sequence to the degenerated sequences of Alu element containing mRNAs should allow the specific detection of those mRNAs in live cells, at least for abundantly expressed mRNAs.

Taken together, the most promising MBs with low F_{back} and high sensitivity had a four G:C base pair stem. Furthermore, the affinity to the target sequences was strongly reduced when eight or six mismatches in the 32 nucleotide long target sequence were present, which is also reflected by a higher ΔG values (Figure 6B) for the base pairing.

Several methods for MB delivery into cells have been established such as electroporation or microinjection (Bratu et al. 2003; Chen et al. 2011; Mao et al. 2020b,), membrane pore formation by streptolysine (Santangelo et al. 2004), and attachment of cell permeable peptides to MBs (Alexander et al. 2011; Nitin and Bao 2008; Nitin et al. 2004). Often high MB concentrations (range of 0.2–5 μM) are used for cell delivery (Chen et al. 2011; Lorenz et al. 2000; Mao et al. 2020b; Nitin et al. 2004). After cellular uptake MBs reach first the cytoplasm and might shuttle between the cytoplasmn and the nucleus as observed for antisense oligonucleotides (Lorenz et al. 2000). As others (Bohlander et al. 2016; Nitin et al. 2004), we used lipid-based transfection reagent RNAiMax for the transfection of MBs. When considering background fluorescence, potentially caused by MB degradation in late endosomes (Nitin et al. 2004) or destabilization of the MB stem (due to ion concentrations, pH), appearance of artificial bright spots and cell survival, the transfection of MBs with a final concentration of 12.5 nM applying RNAiMAX was most appropriate for live cell imaging in chamber slides with glass bottoms.

Live cell microscopy on MB transfected cells, reiterate the *in vitro* data shown herein. Molecular Beacons not expected to have an endogenous target RNA (MBcon), or with reduced complementary to the target, or with stable stems were not opened in cells. We also transfected higher concentration of MBs (75 nM and 100 nM) and observed an increase in background fluorescence and bright signals on cells and in areas without cells, suggesting the formation of lipid:MB complexes causing unspecific MB opening and light emission (data not shown).

In contrast, the MB7SL, MBsnc7SL and MB6145-S directed against endogenous target sequences representing 7SL RNA, snc7SL RNA and piR-has-6145, respectively, were efficiently opened and gave specific fluorescence signals in different cellular compartments, correlating with the known ER location of 7SL RNA in the cytoplasmic SRPs. Furthermore, although containing the 100 % complementary sequence to snc7SL RNA, MBsnc7SL-S was not opened in cells as expected from *in vitro* data showing that even a 5-fold increase in target concentration was not causing an opening of MBsnc7SL-S due to its increased stem stability. This data highlight the importance of initial intensive testing of MBs of different stability and structure *in vitro*.

The comparison of the fluorescence signals of MB7SL and MBsnc7SL show that the endogenous target molecules 7SL RNA and snc7SL RNA have a different cellular localization. Whereas the main MB7SL signal was recorded in cytoplasmic ER regions nearby the nucleus, the main MBsnc7SL signal was found in the nucleus (Figure 9). Since 7SL RNA is the structural component of the signal recognition particle (SRP) it was anticipated that the MB7SL signal overlaps with the signal of the ER staining (Figure 9). MBsnc7SL not only gave a signal in the nucleus but also a faint signal in cytoplasmic region partially overlapping with the MB7SL signal, suggesting that MBsnc7SL also detects 7SL RNA accumulated in the ER (Figure 9C and D). Hence, we cannot rule out that the MBsnc7SL detects 7SL RNA to a low degree. 7SL RNA, an RNA polymerase III transcript is transcribed in the nucleolus and assembles with SRP proteins in the nucleus before being exported to the cytoplasm (Keenan et al. 2001). Because we were only recording a low MB7SL signal in the nucleus (Figure 9C and D), we conclude that the nuclear 7SL RNA concentration is either too low to be detected by MBsnc7SL or that, because of

intensive folding and association with SRP proteins in the nucleus, 7SL RNA is not readily accessible to MBsnc7SL. In contrast, small snc7SL RNA folds also into a structure (ΔG = –6.38 kcal/mol) but not nearly as complex as the 300 nt long 7SL RNA (ΔG = –135.30 kcal/mol, http://www.unafold.org/ (Zuker 2003)). Hence, free snc7SL RNA is presumably more accessible for MBsnc7SL compared to the target sequence buried in the SRP particle. Furthermore, the MBs are highly specific and it is likely that the cytoplasmic MBsnc7SL signal is caused by binding to 7SL RNA or sncRNA7SL. To explain the minor colocalization of the MB7SL and MBsnc7SL signal in the cytoplasm we consider that the high cytoplasmic 7SL RNA concentration allows MBsnc7SL to access enough 7SL RNA molecules to create a signal or that, for a yet unknown reason, sncRNA7SL localizes to the ER. In addition, we consider that it is very likely that sncRNA7SL is associated with RNA-binding proteins such as cytoplasmic Argonaut clade proteins, Hence, it would be interesting to study the colocalization of endogenous sncRNA7SL with Argonaut proteins in the future.

As previously reported the 7SL RNA assembles with the viral Gag protein forming particles at the cell membrane as visualized by applying the MS2 system, in which four binding sites for the MS2 protein were introduced in the S-domain of the 7SL RNA (Itano et al. 2018). This is a very powerful approach for localization and trafficking studies, especially regarding low-expressed RNA. However, it has the limitation that the structure of the RNA or the assembly with SRP proteins, in this case SRP 19, might be impaired.

The nuclear localization of snc7SL RNA leads to interesting questions. For example, we do not know yet the biogenesis pathway of snc7SL RNA, but we speculate that the nuclear microprocessor complex consisting of Drosha and DGCR8 is involved. We can envision that either a certain fraction of abundant native nuclear 7SL RNA is misfolded or that under specific cellular conditions the appropriate association with SRP proteins is disturbed, making 7SL RNA accessible to the microprocessor complex. Whether those 7SL RNA products are exported to the cytoplasm and processed further by Dicer, or whether they stay in the nucleus, is an interesting question. In case that 7SL RNA-derived snc7SL RNA are exported to the cytoplasm, similar to the biogenesis of pre-tRNA derived miRNA mir-1983 (Hasler et al. 2016), the 32 nts long snc7SL RNA might associate with Ago clade proteins forming snc7SL RNPs, similar to DR2 Alu repeat-induced small RNAs (riRNAs) derived from DR2 Alu repeats (Hu et al. 2012).

In conclusion, we established that MB7SL and MBsnc7SL detected their target sequences specifically and revealed a different sub-cellular localization of 7SL RNA and snc7SL RNA. Future studies might uncover the biogenesis of snc7SL RNA and decipher a biological function of this 7SL RNA-derived sncRNA.

4 Materials and methods

4.1 DNA and RNA oligonucleotides and Molecular Beacon (MB)

All DNA oligonucleotides were purchased from (Integrated DNA Technology (IDT)) and all RNA oligonucleotides from Horizone/Dharmafect.

Target RNA oligonucleotides:

RNA modifications: * = Phosphorothioate bond, m = 2′-O-methylation of RNA bases, P = phosphate

snc7SL-target RNA (32 nts):

5′-P-rA*rG*rC*rC*rU*rG*rA*rG*rC*rA*rA*rC*rA*rU*rA*rG*rC*rG*rA*rG*rA*rC

*rC*rC*rC*rG*rU*rC*rU*rC*rU*mA-3′

con-target RNA (32 nts):

5′-P-rA*rU*rC*rU*rC*rU*rC*rC*rU*rG*rC*rC*rC*rC*rC*rA*rG*rA*rG*rC*rG*rA*rU*rA*rC*rA

*rA*rC*rG*rA*rG*rU*rC*rC*rG*mA-3′

Target DNA oligonucleotides:

snc7SL-target DNA (wildtype target sequence):

5′-AGCCTGAGCAACATAGCGAGACCCCGTCTCTA-3′

7SL-target DNA (wildtype target sequence):

5′-AGTTCTGGGCTGTAGTGCGCTATGCCGATC-3′

Degenerated target sequences for snc7SL RNA located in the 3′ UTR of specific mRNAs (mismatches, extra nucleotides or deletions when compared to the wildtype target sequence are shown underlined and as capital, bold letters):

Mdm2: 5′-**-**gc**T**t**AG**g**AG**aca**G**a**TG**gag-**A**c**TT**gtctct**-**

Mdm4-S1: 5′-agcctga**C**c**G**acat**G**g**A**ga**A**accccc**A**t**T**t**T**ta

Mdm4-S2: 5′-agcctg**G**gcaaca**A**tagcga**A**a-c**T**gtctc-a

eEF2K-S1: 5′-agcctg**G**g**T**aa**A**cat**G**gcgagaccc**T**gtctct**-**

eEF2K-S2: 5′-agcctg**G**gc**G**aca**G**ag**T**gagac**T**ccgtctc**G-**

KNL1: 5′-agcctg**G**gcaacat**G**gc**A**a**A**accccc**AC**ctcta

Molecular Beacon (MB) specifications:

FAM = fluorescein: excitation peak at 493 nm, emission peak at 517 nm

DAB = Dabcyl, quenching range: 400–550 nm

Cy5 = Cyanine 5: excitation peak at 651 nm, emission peak at 670 nm

BHQ2 = Black Hole Quencher 2, quenching range: 520–650 nm

MB-snc7SL:

5′-FAM-cgcgAGAGACGGGGTCTCGCTATGTTGCTCAGGCTcgcg-DAB-3′

MB-snc7SL-S:

5′-FAM-cgcgcgAGAGACGGGGTCTCGCTATGTTGCTCAGGCTcgcgcg-DAB-3′

MB-snc7SL-Mut (grey indicate nucleotide deletions or changes (small letters) when compared to wildtype snc7SL RNA):

5′FAM-cgcgca—ACGGGGTaTCGaTATGTTGCTCAGGC-agcgcg-DAB-3′

MBcon:

5′FAM-cgcgTCGGACTCGTTGTATCGCTCTGGGGCAGAGATcgcg-DAB-3′

MBcon-S:

5′FAM-cgcgcgTCGGACTCGTTGTATCGCTCTGGGGCAGAGATcgcgcg-DAB-3′

MB7SL:
5′Cy5-cgcgaGATCGGCATAGCGCACTACAGCCCAGAACTcgcg-BHQ2-3′
MB6145-S:
5′Fam-cgcgcgTGAGGCGAACGTGATAACCACTACACTACGGAcgcgcg-D-3′

4.2 *In vitro* Molecular Beacon (MB) assay

All reactions (20 µL) were performed in 384-well black plates (Perkin Elmer) and fluorescence was recorded over time at 37 °C in a BMG Caliber instrument (gain set at 1000). All reagents and 384-well plates were cooled on ice. Reactions comprised of MBs and target RNA or DNA oligonucleotides were assembled on ice in 1× ICN buffer (10 mM Tris/HCl, pH 7.5, 100 mM KCl, 10 mM NaCl, 0.75 mM $MgCl_2$, 0.0001 % NP40) and transferred to the pre-warmed (37 °C) multiplate reader.

4.3 Cells and cell culture

SK–N–SH and U2–OS cells were expanded and aliquots were stored in liquid nitrogen. New cell cultures were established every 2–3 months. SK–N–SH and U2–OS cells were purchased from DSMZ (German Collection of Microorganisms and Cell Cultures GmbH). SK–N–SH cells were cultured EMEM/Ham's F12 (1:1) medium with 10 % fetal bovine serum, 2 mM glutamine, 1 % penicillin/streptomycin. U2–OS cells were cultured in RPMI with 10 % fetal bovine serum, 4 mM glutamine, 1 % penicillin/streptomycin.

4.4 Transfection of Molecular Beacons using RNAiMax

Molecular Beacons (MB) were transfected using the Lipofectamine RNAiMAX Transfection Reagent (ThermoFisher Scientific, #13778030).

For live-cell imaging with the Bio-Rad ZOE cell imager 24-Well plates were used. For a single transfection 100 µM MB stock solutions were diluted to 1 µM in H_2O and further diluted to 125 nM in 50 µL Opti-MEM. Furthermore, 1 µL Lipofectamine RNAiMAX was mixed with 49 µL Opti-MEM in a second Eppendorf tube. Contents of both tubes were mixed together and incubated at room temperature for 5 min. Afterwards transfection solution was mixed with 400 µL of medium containing between 50,000 and 150,000 U2–OS cells. Cells and transfection solution were mixed by pipetting and plated into one 24-Well plates. Final MB concentration 12.5 nM.

For live-cell imaging with the KEYENCE BZ-X810 fluorescence microscope 30,000 cells were plated into µ-slide 8 well chambered coverslip (Ibidi, #80826) and either cultured for 24 h prior to transfection at 37 °C in 5 % CO_2 atmosphere in medium (pre-plated) or mixed directly with the transfection mix and plated.

For a single transfection MB stocks (100 µM) were diluted to 1 µM in H_2O and further diluted in Opti-MEM (Life Technologies #11058021) to a concentration of 125 nM, 250 nM, 500 nM, 750 nM and 1 µM in 30 µL. In a second Eppendorf tube, 0.6 µL RNAiMAX was mixed with 29.4 µL Opti-MEM. All contents were thoroughly mixed by pipetting. The liquids of the two Eppendorf tubes were combined, mixed thoroughly by pipetting and incubated for 5 min at room temperature, resulting in concentrations of 62.5 nM, 125 nM, 250 nM, 375 nM and 500 nM. Finally, 60 µL transfection mix was mixed with 240 µL medium and added to one well of pre-plated cells. Final MB concentrations are 12.5 nM, 25 nM, 50 nM, 75 nM or 100 nM.

Cells were cultured for 24 h at 37 °C in a humified incubator set to 5 % CO_2 atmosphere. Subsequently cells were washed once with 1× PBS (Life Technologies #14190-169), stained with DAPI (diluted 1 drop per mL in PBS, Thermos Fisher #R37605,) and incubated for 10 min at room temperature. Next the DAPI solution was replaced with 1× PBS and cells were washed once with 1× PBS. Finally, cells were covered with 300 µL 1× PBS and analyzed by fluorescence microscopy using the KEYENCE (BZ-X810) microscope or the Leica TCS SP5 confocal laser scanning microscope. In case of live-cell imaging with the Bio-Rad ZOE cell imager cells were not stained with DAPI.

4.5 Cell imaging and fluorescence microscopy

For live cell imaging with a Bio-Rad ZOE cell imager, a brightfield channel, a green channel (excitation: 480/17 nm; emission: 517/23 nm) and a LED light source was used. Live cell images were taken with a KEYENCE BZ-X810 fluorescence microscope equipped with a LED light source. Exposure times of 1/35 s to 3 s and magnifications between 20× (Objective: Plan Fluor 20× Na 0.45×), 40× (Objective: Plan Apo 40× NA 0.95×) and 100× (Objective: Plan Apo 100× 1.45, Oil) were applied. The following filters were used: BZ-X filter GFP (excitation 470 nM; emission 525 nM); BZ-X filter Cy5 (excitation 620 nM; emission 700 nM), BZ-X filter DAPI (excitation 360 nM; emission 460 nM). Z-stacks in the range of 0.2–0.8 µM were generated and line profiles were created by using the KEYENCE measurement module. For background signal adjustment, untransfected cells or control (MBcon) transfected cells were imaged. Exposure times were set so that control cells do not provide any signal. For data analysis, the BZ-X800 Analyzer software package (Version 1.1.2.4) was used.

The Leica TCS SP5 confocal laser scanning microscope with a laser as light source (Argon ion laser for 458 nm, 476 nm, 488 nm, 496 nm, 514 nm; Helium–neon laser for 633 nm; Diode laser for 561 nm and Pulsed UV laser (including B&H control system)) was used for live-cell imaging as well. Magnification of 40× (oil) and 63× (oil) were applied. Lasers were set on a range of 470 nM–525 nM for FAM detection, on a range of 620 nM–700 nM for Cy5 detection and on a range of 360 nM–460 nM for DAPI detection, respectively. Z-stacks were generated. For background signal adjustment, untransfected cells or control (MBcon) transfected cells were imaged. Exposure times were set so that control cells do not provide any signal. Pictures were processed with the Leica Application Suite (Version 2.7.3.9723) and with the Adobe software package Elements.

4.6 Staining of the endoplasmic reticulum (ER)

ER Tracker Green 100 µg, Thermo fisher #E34251, dye BODIPY® FL (EX/EM 504/511) was dissolved in 128 µL DMSO upon arrival to a concentration of 1 mM. ER Tracker Green Stock solution (1 mM) was diluted to 100 nM in 1× PBS and 300 µL were added to the cells and incubated for 20 min at 37 °C. Thereafter, the liquid was replaced with fresh 1× PBS and pictures were taken with the KEYENCE BZ-X810 fluorescence microscope using the BZ-X filter GFP (excitation 470 nM; emission 525 nM).

Acknowledgments: We thank Prof. Dr. Bernhard Weber (Institute of Human Genetics and Institute of Clinical Human Genetics, University of Regensburg, Germany) and Prof. Dr. Andre Gessner (Institute of Microbiology and Hygiene, University Hospital Regensburg, Germany) for access to the Keyence and the Confocal microscopes, respectively.

Research ethics: Not applicable.

Author contributions: All the authors have accepted responsibility for the entire content of this submitted manuscript and approved submission.

Conflict of interest: The authors declare no conflicts of interest regarding this article.

Research funding: This work was funded by the German Research Association Deutsche Forschungsgemeinschaft (DFG) [SFB 960/3, project B14], which is gratefully acknowledged.

Data availability: The raw data can be obtained on request from the corresponding author.

References

Alexander, J.C., Pandit, A., Bao, G., Connolly, D., and Rochev, Y. (2011). Monitoring mRNA in living cells in a 3D *in vitro* model using TAT-peptide linked molecular beacons. Lab Chip 11: 3908–3914.

Andersen, E.S., Rosenblad, M.A., Larsen, N., Westergaard, J.C., Burks, J., Wower, I.K., Wower, J., Gorodkin, J., Samuelsson, T., and Zwieb, C. (2006). The tmRDB and SRPDB resources. Nucleic Acids Res. 34: D163–D168.

Basilio Barbosa, V., De Oliveira Martins, E., and Weber, G. (2019). Nearest-neighbour parameters optimized for melting temperature prediction of DNA/RNA hybrids at high and low salt concentrations. Biophys. Chem. 251: 106189.

Bohlander, P.R., Abba, M.L., Bestvater, F., Allgayer, H., and Wagenknecht, H.A. (2016). Two wavelength-shifting molecular beacons for simultaneous and selective imaging of vesicular miRNA-21 and miRNA-31 in living cancer cells. Org. Biomol. Chem. 14: 5001–5006.

Bonnet, G., Tyagi, S., Libchaber, A., and Kramer, F.R. (1999). Thermodynamic basis of the enhanced specificity of structured DNA probes. Proc. Natl. Acad. Sci. U. S. A. 96: 6171–6176.

Bovia, F. and Strub, K. (1996). The signal recognition particle and related small cytoplasmic ribonucleoprotein particles. J. Cell Sci. 109: 2601–2608.

Bratu, D.P., Cha, B.J., Mhlanga, M.M., Kramer, F.R., and Tyagi, S. (2003). Visualizing the distribution and transport of mRNAs in living cells. Proc. Natl. Acad. Sci. U. S. A. 100: 13308–13313.

Chen, A.K., Rhee, W.J., Bao, G., and Tsourkas, A. (2011). Delivery of molecular beacons for live-cell imaging and analysis of RNA. Methods Mol. Biol. 714: 159–174.

Cole, C., Sobala, A., Lu, C., Thatcher, S.R., Bowman, A., Brown, J.W., Green, P.J., Barton, G.J., and Hutvagner, G. (2009). Filtering of deep sequencing data reveals the existence of abundant Dicer-dependent small RNAs derived from tRNAs. RNA 15: 2147–2160.

Consortium, R.N., Petrov, A.I., Ribas, C.E., Finn, R.D., Bateman, A., Szymanski, M., Karlowski, W.M., Seemann, S.E., Gorodkin, J., Cannone, J.J., et al. (2021). RNAcentral 2021: secondary structure integration, improved sequence search and new member databases. Nucleic Acids Res. 49: D212–D220.

Czech, B. and Hannon, G.J. (2016). One loop to rule them all: the ping-pong cycle and piRNA-guided silencing. Trends Biochem. Sci. 41: 324–337.

De Marco Zompit, M. and Stucki, M. (2021). Mechanisms of genome stability maintenance during cell division. DNA Repair (Amst) 108: 103215.

Dieci, G., Fiorino, G., Castelnuovo, M., Teichmann, M., and Pagano, A. (2007). The expanding RNA polymerase III transcriptome. Trends Genet. 23: 614–622.

Ferreira, I., Jolley, E.A., Znosko, B.M., and Weber, G. (2019). Replacing salt correction factors with optimized RNA nearest-neighbour enthalpy and entropy parameters. Chem. Phys. 521: 69–76.

Fish, L., Zhang, S., Yu, J.X., Culbertson, B., Zhou, A.Y., Goga, A., and Goodarzi, H. (2018). Cancer cells exploit an orphan RNA to drive metastatic progression. Nat. Med. 24: 1743–1751.

Gruber, A.R., Lorenz, R., Bernhart, S.H., Neubock, R., and Hofacker, I.L. (2008). The Vienna RNA websuite. Nucleic Acids Res. 36: W70–W74.

Ha, M. and Kim, V.N. (2014). Regulation of microRNA biogenesis. Nat. Rev. Mol. Cell Biol. 15: 509–524.

Hashim, A., Rizzo, F., Marchese, G., Ravo, M., Tarallo, R., Nassa, G., Giurato, G., Santamaria, G., Cordella, A., Cantarella, C., et al. (2014). RNA sequencing identifies specific PIWI-interacting small non-coding RNA expression patterns in breast cancer. Oncotarget 5: 9901–9910.

Hasler, D. and Meister, G. (2016). From tRNA to miRNA: RNA-folding contributes to correct entry into noncoding RNA pathways. FEBS Lett. 590: 2354–2363.

Hasler, D., Lehmann, G., Murakawa, Y., Klironomos, F., Jakob, L., Grasser, F.A., Rajewsky, N., Landthaler, M., and Meister, G. (2016). The Lupus autoantigen La prevents mis-channeling of tRNA fragments into the human MicroRNA pathway. Mol. Cell 63: 110–124.

Hock, J. and Meister, G. (2008). The Argonaute protein family. Genome Biol. 9: 210.

Hu, Q., Tanasa, B., Trabucchi, M., Li, W., Zhang, J., Ohgi, K.A., Rose, D.W., Glass, C.K., and Rosenfeld, M.G. (2012). DICER- and AGO3-dependent generation of retinoic acid-induced DR2 Alu RNAs regulates human stem cell proliferation. Nat. Struct. Mol. Biol. 19: 1168–1175.

Intine, R.V., Sakulich, A.L., Koduru, S.B., Huang, Y., Pierstorff, E., Goodier, J.L., Phan, L., and Maraia, R.J. (2000). Control of transfer RNA maturation by phosphorylation of the human La antigen on serine 366. Mol. Cell 6: 339–348.

Itano, M.S., Arnion, H., Wolin, S.L., and Simon, S.M. (2018). Recruitment of 7SL RNA to assembling HIV-1 virus-like particles. Traffic 19: 36–43.

Iwakawa, H.O. and Tomari, Y. (2022). Life of RISC: formation, action, and degradation of RNA-induced silencing complex. Mol. Cell 82: 30–43.

Izumi, N., Shoji, K., Suzuki, Y., Katsuma, S., and Tomari, Y. (2020). Zucchini consensus motifs determine the mechanism of pre-piRNA production. Nature 578: 311–316.

Jurka, J. (2004). Evolutionary impact of human Alu repetitive elements. Curr. Opin. Genet. Dev. 14: 603–608.

Keenan, R.J., Freymann, D.M., Stroud, R.M., and Walter, P. (2001). The signal recognition particle. Annu. Rev. Biochem. 70: 755–775.

Kostrikis, L.G., Tyagi, S., Mhlanga, M.M., Ho, D.D., and Kramer, F.R. (1998). Spectral genotyping of human alleles. Science 279: 1228–1229.

Kota, V., Sommer, G., Hazard, E.S., Hardiman, G., Twiss, J.L., and Heise, T. (2018). SUMO modification of the RNA-binding protein La regulates cell proliferation and STAT3 protein stability. Mol. Cell. Biol. 38: 1–16.

Kuehnert, J., Sommer, G., Zierk, A.W., Fedarovich, A., Brock, A., Fedarovich, D., and Heise, T. (2015). Novel RNA chaperone domain of RNA-binding protein La is regulated by AKT phosphorylation. Nucleic Acids Res. 43: 581–594.

Kuksa, P.P., Amlie-Wolf, A., Katanic, Z., Valladares, O., Wang, L.S., and Leung, Y.Y. (2019). DASHR 2.0: integrated database of human small non-coding RNA genes and mature products. Bioinformatics 35: 1033–1039.

Kumar, P., Kuscu, C., and Dutta, A. (2016). Biogenesis and function of transfer RNA-related fragments (tRFs). Trends Biochem. Sci. 41: 679–689.

Leung, Y.Y., Kuksa, P.P., Amlie-Wolf, A., Valladares, O., Ungar, L.H., Kannan, S., Gregory, B.D., and Wang, L.S. (2016). DASHR: database of small human noncoding RNAs. Nucleic Acids Res. 44: D216–D222.

Liang, C., Xiong, K., Szulwach, K.E., Zhang, Y., Wang, Z., Peng, J., Fu, M., Jin, P., Suzuki, H.I., and Liu, Q. (2013). Sjogren syndrome antigen B (SSB)/La promotes global microRNA expression by binding microRNA precursors through stem-loop recognition. J. Biol. Chem. 288: 723–736.

Liu, Y., Tan, H., Tian, H., Liang, C., Chen, S., and Liu, Q. (2011). Autoantigen La promotes efficient RNAi, antiviral response, and transposon silencing by facilitating multiple-turnover RISC catalysis. Mol. Cell 44: 502–508.

Lorenz, P., Misteli, T., Baker, B.F., Bennett, C.F., and Spector, D.L. (2000). Nucleocytoplasmic shuttling: a novel *in vivo* property of antisense phosphorothioate oligodeoxynucleotides. Nucleic Acids Res. 28: 582–592.

Mao, S., Ying, Y., Wu, R., and Chen, A.K. (2020a). Recent advances in the molecular beacon technology for live-cell single-molecule imaging. iScience 23: 101801.

Mao, S., Ying, Y., Wu, X., and Chen, A.K. (2020b). Delivering molecular beacons via an electroporation-based approach enables live-cell imaging of single RNA transcripts and genomic loci. Methods Mol. Biol. 2106: 241–252.

Maraia, R.J., Mattijssen, S., Cruz-Gallardo, I., and Conte, M.R. (2017). The La and related RNA-binding proteins (LARPs): structures, functions, and evolving perspectives. Wiley Interdiscip. Rev. RNA 8: e1430.

Megel, C., Morelle, G., Lalande, S., Duchene, A.M., Small, I., and Marechal-Drouard, L. (2015). Surveillance and cleavage of eukaryotic tRNAs. Int. J. Mol. Sci. 16: 1873–1893.

Naim, V. and Rosselli, F. (2009). The FANC pathway and BLM collaborate during mitosis to prevent micro-nucleation and chromosome abnormalities. Nat. Cell Biol. 11: 761–768.

Nakano, S., Fujimoto, M., Hara, H., and Sugimoto, N. (1999). Nucleic acid duplex stability: influence of base composition on cation effects. Nucleic Acids Res. 27: 2957–2965.

Nitin, N. and Bao, G. (2008). NLS peptide conjugated molecular beacons for visualizing nuclear RNA in living cells. Bioconjug. Chem. 19: 2205–2211.

Nitin, N., Santangelo, P.J., Kim, G., Nie, S., and Bao, G. (2004). Peptide-linked molecular beacons for efficient delivery and rapid mRNA detection in living cells. Nucleic Acids Res. 32: e58.

Ozata, D.M., Gainetdinov, I., Zoch, A., O'Carroll, D., and Zamore, P.D. (2019). PIWI-interacting RNAs: small RNAs with big functions. Nat. Rev. Genet. 20: 89–108.

Pekarsky, Y., Balatti, V., and Croce, C.M. (2023). tRNA-derived fragments (tRFs) in cancer. J. Cell Commun. Signaling 17: 47–54.

Pippadpally, S. and Venkatesh, T. (2020). Deciphering piRNA biogenesis through cytoplasmic granules, mitochondria and exosomes. Arch. Biochem. Biophys. 695: 108597.

Quentin, Y. (1994). A master sequence related to a free left Alu monomer (FLAM) at the origin of the B1 family in rodent genomes. Nucleic Acids Res. 22: 2222–2227.

Roy, J. and Mallick, B. (2018). Investigating piwi-interacting RNA regulome in human neuroblastoma. Genes Chromosomes Cancer 57: 339–349.

Santangelo, P.J., Nix, B., Tsourkas, A., and Bao, G. (2004). Dual FRET molecular beacons for mRNA detection in living cells. Nucleic Acids Res. 32: e57.

Schwartz, E.I., Intine, R.V., and Maraia, R.J. (2004). CK2 is responsible for phosphorylation of human La protein serine-366 and can modulate rpL37 5′-terminal oligopyrimidine mRNA metabolism. Mol. Cell. Biol. 24: 9580–9591.

Shibata, Y., Voeltz, G.K., and Rapoport, T.A. (2006). Rough sheets and smooth tubules. Cell 126: 435–439.

Sommer, G. and Heise, T. (2021). Role of the RNA-binding protein La in cancer pathobiology. RNA Biol. 18: 218–236.

Treiber, T., Treiber, N., and Meister, G. (2019). Regulation of microRNA biogenesis and its crosstalk with other cellular pathways. Nat. Rev. Mol. Cell Biol. 20: 5–20.

Tyagi, S. and Kramer, F.R. (1996). Molecular beacons: probes that fluoresce upon hybridization. Nat. Biotechnol. 14: 303–308.

Tyagi, S., Bratu, D.P., and Kramer, F.R. (1998). Multicolor molecular beacons for allele discrimination. Nat. Biotechnol. 16: 49–53.

Van Niekerk, E.A., Willis, D.E., Chang, J.H., Reumann, K., Heise, T., and Twiss, J.L. (2007). Sumoylation in axons triggers retrograde transport of the RNA-binding protein La. Proc. Natl. Acad. Sci. U. S. A. 104: 12913–12918.

Wang, J., Shi, Y., Zhou, H., Zhang, P., Song, T., Ying, Z., Yu, H., Li, Y., Zhao, Y., Zeng, X., et al. (2022). piRBase: integrating piRNA annotation in all aspects. Nucleic Acids Res. 50: D265–D272.

Weber, G. (2015). Optimization method for obtaining nearest-neighbour DNA entropies and enthalpies directly from melting temperatures. Bioinformatics 31: 871–877.

Wolin, S.L. and Cedervall, T. (2002). The La protein. Annu. Rev. Biochem. 71: 375–403.

Yamasaki, S., Ivanov, P., Hu, G.F., and Anderson, P. (2009). Angiogenin cleaves tRNA and promotes stress-induced translational repression. J. Cell Biol. 185: 35–42.

Zhang, X.O., Pratt, H., and Weng, Z. (2021). Investigating the potential roles of SINEs in the human genome. Annu. Rev. Genomics Hum. Genet. 22: 199–218.

Zuker, M. (2003). Mfold web server for nucleic acid folding and hybridization prediction. Nucleic Acids Res. 31: 3406–3415.

Supplementary Material: This article contains supplementary material (https://doi.org/10.1515/hsz-2023-0185).